Decoding Muscle Force From Motor Unit Firings Using Encoder-Decoder Networks

Xiao Tang, *Student Member, IEEE*, Xu Zhang, *Member, IEEE*, Maoqi Chen, Xiang Chen, *Member, IEEE*, and Xun Chen, *Senior Member, IEEE*

***Abstract*— Appropriate interpretation of motor unit (MU) activities after surface EMG (sEMG) decomposition is a key factor to decode motor intentions in a noninvasive and physiologically meaningful way. However, there are great challenges due to the difficulty in cross-trial MU tracking and unavoidable loss of partial MU information resulting from incomplete decomposition. In light of these issues, this study presents a novel framework for interpreting MU activities and applies it to decode muscle force. The resulting MUs were clustered and classified into different categories by characterizing their spatially distributed firing waveforms. The process served as a general MU tracking method. On this basis, after transferring the MU firing trains to twitch force trains by a twitch force model, a deep network was designed to predict the normalized force. In addition, MU category distribution was examined to calibrate the actual force level, while functions of some unavailable MUs were compensated. To investigate the effectiveness of this framework, high-density sEMG signals were recorded using an 8 $\times$ 8 electrode array from the abductor pollicis brevis muscles of eight subjects, while thumb abduction force was measured. The proposed method outperformed three common methods ($p < 0.001$) yielding the lowest root mean square deviation of 6.68% $\pm$ 1.29% and the highest fitness (R^2) of 0.94 $\pm$ 0.04 between the predicted force and the actual force. This study offers a valuable, computational solution for interpreting individual MU activities, and its effectiveness was confirmed in muscle force estimation.**

***Index Terms*— Muscle force estimation, EMG decomposition, neural drive information, motor unit, deep learning.**

I. Introduction

THERE is a great demand for natural and effective human-machine interfaces, facing major challenges in accurately decoding motor intentions from biological signals collected from the brain, peripheral nerves, and muscles [1]–[3]. Surface electromyography (sEMG) directly reflects muscle activities of related motor intentions [4] and contains both pattern [5], [6] and strength [7], [8] information thereof. It also possesses an easy-to-use advantage with non-invasive measurements [9]. Therefore, it has become a common technique for extracting neural commands and decoding motor intentions.

The basic goal of decoding motor intentions is to decode the motor strength, which is also known as muscle force estimation. Generally, previous studies into the muscle force estimation mainly employed various features in the time-, frequency-, or nonlinear domains of the sEMG signals [10]–[14]. Of these, amplitude-associated features such as root mean square (RMS) of amplitude [10], [11] and envelop (ENV) have attracted many research interests with development of numerous computational models or optimization methods to boost their performance [12], [14]. However, these methods mainly depend on data-driven statistical models rather than the physiological nature of muscle force generation. Due to severe overlap of individual MUs' activities, coupling of noises and cross-talks from multiple muscles in the raw sEMG signals, these macroscopic features can only offer a general interpretation of muscle force with limited precision.

Recently, sEMG decomposition has become a rapidly developing technique [15]–[18], [44]–[47] that can break down the highly superposed sEMG signals into its constituting components, i.e., motor unit (MU) activities, primarily using blind source separation algorithms. Those acquired MU activities are regarded as a direct reflection of microscopic neural drive information and serve as a practical way to accurately decode motor intentions, and the muscle force in particular [19]–[24]. Many studies made use of the discharge timings of all decomposed MUs to estimate the muscle force [22], [23]. A few studies have tried to roughly discriminate contributions for individual MUs by employing an MU twitch model to assign numerical contributions in the order of their recruitment [24]. These studies have preliminarily verified the feasibility of estimating muscle force from MU activities. However, given the limited performance of the cutting-edge sEMG decomposition technique, it is still very difficult to easily interpret and utilize these individual MU activities towards precise decoding of muscle force.

After sEMG decomposition, the difficulty in cross-trial MU tracking and unavoidable loss of partial MU information due to incomplete decomposition [43], [44] emerge as two

Manuscript received November 2, 2020; revised April 16, 2021 and August 29, 2021; accepted October 27, 2021. Date of publication November 8, 2021; date of current version December 10, 2021. This work was supported in part by the National Natural Science Foundation of China under Grant 61771444 and in part by the Guangzhou Science and Technology Program under Grant 201704030039. *(Corresponding author: Xu Zhang.)*

This work involved human subjects or animals in its research. Approval of all ethical and experimental procedures and protocols was granted by the Ethics Review Committee of the University of Science and Technology of China, Hefei, Anhui, China, under Approval No. PJ2017-04-06.

Xiao Tang, Xu Zhang, Xiang Chen, and Xun Chen are with the School of Information Science and Technology, University of Science and Technology of China, Hefei, Anhui 230026, China (e-mail: xuzhang90@ustc.edu.cn).

Maoqi Chen is with the Institute of Rehabilitation Engineering, University of Health and Rehabilitation Sciences, Qingdao, Shandong 266072, China.

Digital Object Identifier 10.1109/TNSRE.2021.3126752

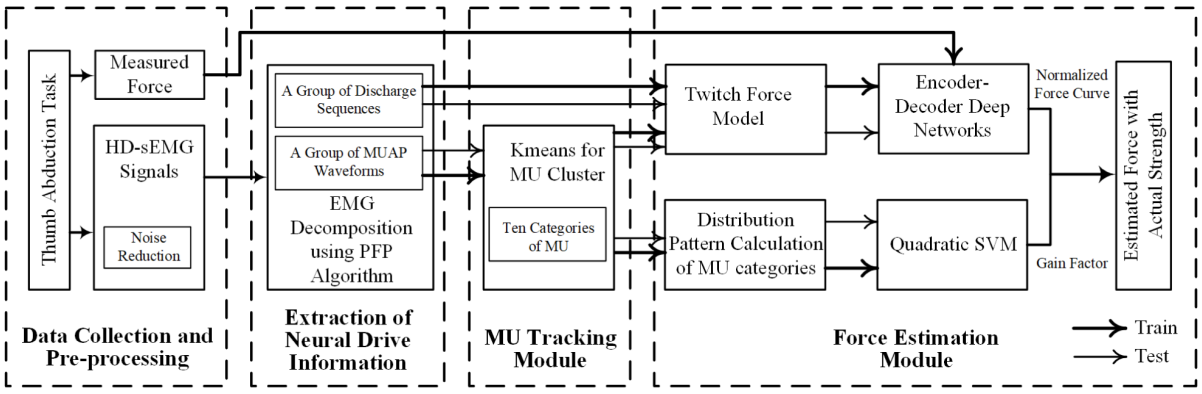

Fig. 1. Block diagram of the proposed study framework. Two modules were well designed to address the issues in applications of EMG decomposition. The MU tracking module recognized the MUs by a clustering operation. The force estimation module employed machine learning algorithms to decode the muscle force from the representative subset of MUs.

key issues that restrict its wide applications. Induced by the blind source separation algorithms, although the raw high density sEMG (HD-sEMG) signals can be decomposed into a set of activated MUs, their number was uncertain with no knowledge of their type and size when the decomposition was performed across trials (i.e., each segment of EMG signal is decomposed individually). Thus, it brings a great challenge to accurately track all decomposed MUs across trials, leading to the difficulty in understanding the function of every MU. The other challenge originates from the unavoidable loss of partial MU information due to unsuccessful and incomplete decomposition of all activated MUs. Such incomplete decomposition always presents inconsistent and unknown degrees of decomposition leading to slight or considerable differences between two groups of MUs in number and type when they are decomposed separately. These differences restrict the use of more advanced techniques such as machine learning or deep learning in the interpretation of MU activities. Therefore, solving these two issues above is a prerequisite for effective interpretation of neural drive information, and it also leads to a key foundation to decode the muscle force.

This study is devoted to developing a novel framework for accurately interpreting MU activities from the sEMG decomposition towards precise force estimation. The entire framework was constructed based on two primary scientific hypotheses. The first hypothesis is that MUs with similar spatial and amplitude characteristics of their MUAP waveforms exhibit more or less the same function (i.e., the force contribution). On this basis, a clustering and classification procedure was designed to generally track the MUs across trials. Second, a group of MUs derived from the sEMG decomposition were further hypothesized to be a representative subset of all activated MUs sufficiently reflecting the dominant neural drives of muscle force. Therefore, it is possible to decode the relatively precise muscle force by generalizing the knowledge learnt from such a representative subset of MUs through a machine learning approach. To verify both hypotheses and to demonstrate the feasibility of the framework, it was applied to muscle force estimation. This study not only presents a tool for predicting muscle force via MU activities, but also provides an efficient and practical solution for interpreting and understanding individual MU's functions and contributions after applying cutting-edge sEMG decomposition techniques.

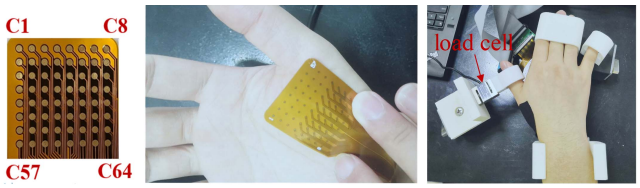

Fig. 2. (a) The proposed electrode array containing 64 metal probes arranged in an 8 × 8 array. (b) The placement of the electrode array. (c) The 3D printed fixtures for fixing the wrists and fingers and the one-dimensional load cell for force measurement.

II. Methods

Fig. 1 shows the proposed framework in this study consisting of three major procedures. Neural drive information in the form of MU activities was extracted using a HD-sEMG decomposition technique. The MU tracking module was designed to roughly recognize different MUs across trials through clustering and then to classify the MUs into some categories. The force estimation module worked in two parallel lines. One line estimated the normalized force curve by quantifying each MU's contribution to the force in every category, and the other line evaluated the MU category distribution pattern to predict the gain factor for obtaining the actual force. Both lines were designed using machine learning approaches incorporated with corresponding known physiological mechanisms.

A. Data Collection and Preprocessing

In this study, eight neurologically intact male subjects without any musculoskeletal injuries or neuromuscular disorders, especially in hand function (age: 24 ± 2, mean ± standard deviation), were recruited. The experimental protocol of this study was approved by the Ethics Review Committee of University of Science and Technology of China (Hefei, Anhui, China). All subjects gave their informed and written consent prior to any procedure of the experiments.

HD-sEMG signals were recorded from the abductor pollicis brevis (APB) muscle on any hand of the subject using a flexible 64-channel mono-polar electrode array arranged in an 8 × 8 grid. Each electrode probe of the array was 2 mm in diameter with an inter-electrode distance of 4 mm. Our home-made multi-channel sEMG data recording system was used. Its reliability has been already validated in previous studies [12], [25]. The recording system was built with a two-stage amplifier at a total gain of 60 dB (AD8200, Analog Devices; OPA349, Texas Instruments), a band-pass filter set at 20-500 Hz for each sEMG channel, and a 16-bit analog-to-digital converter (ADS1198, Texas Instruments). The sampling rate was set at 2 kHz for recording HD-sEMG signals. A one-dimensional load cell (LDST-V-HY, Luckly Inc., Beijing, China) was attached to the recording system for synchronous recording of both the force and HD-sEMG data. A series of 3D-printed apparatuses with magnetic bases were fixed on appropriate positions on the examination table to support the tested hand and to mobilize the wrist and fingers against other movement interference.

After skin preparation using medical alcohol, the electrode array was placed over the APB muscle of the tested hand with all columns of the array along the direction of the thumb. The thumb was put into a round circle attached on the load cell for force recording. The other four fingers and wrist were fixed by customized apparatuses. Before data collection, the maximum voluntary contraction (MVC) of the tested muscle was determined for each subject. The subject was required to perform thumb abduction with maximal effort three times each maintained for at least 2 s. The maximum reading of the force output during the three repetitions was regarded as the MVC.

The following experimental protocol involved four different force levels set at 10%, 20%, 30%, and 40% of the MVC. At each force level, there are five data recording trials by performing the task of thumb abduction with five repetitions. In a single trial, subjects were instructed to gradually increase the muscle force within 2-s until reaching the target force level and then maintain the level for an additional 3 s. A sufficiently long rest was allowed between two consecutive trials and force levels to avoid fatigue. During the experiment, the actual force exerted by the subject was shown on a computer screen in real time as feedback. A pre-defined force curve was also shown on the screen as a target to guide the force generation for each subject. Subjects were encouraged to follow the target curve, but deviation from this curve was allowed during the experiment. Only actual recorded force data were adopted in the follow-up data analysis. The recorded sEMG and force data were transferred to a hard disk for further off-line analyses.

Several steps were taken to reduce the noise contamination in the pre-processing procedure [25]. The recorded sEMG signals were filtered by a Butterworth band-pass filter set at 20-500 Hz to eliminate the potential low-frequency motion artifacts and high-frequency interference. A set of notch filters were utilized to reduce the effect of power line interference as well as its harmonics. A 5-s data segment including the filtered HD-sEMG signals and corresponding force data was extracted from each trial. A total of 20 data segments were obtained over four force levels for each subject.

B. HD-sEMG Decomposition Into Individual MU Activities

HD-sEMG decomposition was used to extract individual MU activities as a physiological representation of neural drives. Due to the superior capability of capturing spatial information, the development of HD-sEMG leads to a significant progress of sEMG decomposition based on blind source separation techniques. Recently, many HD-sEMG decomposition algorithms have emerged and are well-designed. Of these, both convolution kernel compensation (CKC) [18] and progressive FastICA peel-off (PFP) [16], [17] are representative algorithms that have been widely recognized and validated. They were also reported to yield comparable performance [15]. In this study, the PFP algorithm was employed with the consideration that the peel-off strategy enables the ability to extract as more MUs as possible [16], [17]. The PFP can be alternated by other decomposition algorithms such as CKC or other modified versions towards automatic and online decomposition [44]–[47].

C. Module for MU Tracking and Identification

It is possible to obtain different groups of MUs when the sEMG segments were separately decomposed. Therefore, it is necessary to track and identify them across trials. Strict tracking of individual MUs requires to recognize every identical MU across different trials [42], but this is difficult and even impractical to be validated. Alternatively, we adopted a general cross-trial MU tracking strategy that can identify MUs by "category" based on the similarity of spatial distribution patterns of their MUAP waveforms over the 2D electrode array. From muscle physiology experiments, the spatial and amplitude characteristics of the MUAP waveforms are determined by many factors such as the size, type, and location (including depth) of every MU [52]. Specifically, many larger MUs are likely to be distributed at superficial/shallow locations of the muscle thus leading to greater MUAP amplitude and force contribution [53]. Although it is impossible to accurately measure or estimate these factors (depth in particular) of individual MUs from the sEMG, we hypothesized that the MUAP waveform pattern can generally reflect the MU's function and force contribution in this study. This explains the general MU-tracking strategy, which led to an engineering solution for classifying MUs exhibiting similar MUAP waveform patterns into the same category. We further assumed that the MU size was positively correlated with the MUAP amplitude for a population of decomposed MUs. This general and simplified trend was established due to the trade-off between the physiological nature and computational practicability.

There were two procedures in this module: One was an unsupervised learning procedure termed clustering to determine how many and what categories (i.e., clusters) a population of MUs could be divided and placed into. The other was a supervised learning procedure termed classification to identify what category a new MU could belong to, on the basis of a training set of MUs whose category membership was known from the prior clustering procedure. To characterize the

MUAP waveform in each channel, the maximum and absolute value of the minimum and RMS amplitude were calculated as three features. These features from all channels were then concatenated to form a feature vector for each MU.

In the former clustering procedure, a K-means algorithm was applied to cluster the MUs into K categories. It was necessary to pre-assign the number K with a primary criterion to minimize the within-category sum of squared errors (SSE) while K is set as small as possible [29], [30]. The relation between the SSE and K was investigated by some pre-tests, and then K was finally set to 10 in this study. Afterwards, the centroid (a vector in the feature space) of each of 10 categories was calculated via the K-means algorithm. At this stage, there was no information regarding the order of these categories. Considering that the centroid was able to represent each MU category, the norm of the centroid was thus calculated. It was used to represent the size of the MUs belonging to the category according to the above assumption that the MU size was reflected by its MUAP amplitude. Thus, all categories were sorted in an ascending order of their centroid norms. These were then labelled as C1-C10 accordingly. In the subsequent MU classification procedure, it was straightforward to consider the MU categories with centroids determined by the prior clustering procedure as a well-trained classifier. The original population of MUs were clustered into 10 categories and were used as the training dataset of the classification procedure. In the testing phase, any given MU could be identified to belong to one category from whose centroid the MU's feature vector had the minimum Euclidean distance. Therefore, this module provided function of generally tracking and identifying every decomposed MU from each trial with a specific category within C1-C10. This made it possible to properly align the input data, which is beneficial for further analysis such as utilizing deep networks.

D. Module for Decoding Muscle Force With Neural Drive Information From Categorized MUs

The incomplete decomposition of HD-sEMG signals directly led to unavoidable loss of some activated MUs, thus affecting the integrity of the MU activities. This became an important issue in decoding the neural commands producing the muscle force. To address this issue, we further hypothesized that the resulting MUs can be regarded as a sufficiently representative subset of all activated MUs. In order to predict the primary behavior of all activated MUs (i.e., the muscle force production in this study) from the representative subset, two parallel lines were designed with appropriate machine learning algorithms. One line decoded the normalized muscle curve, and the other line predicted a gain factor representing the corresponding force level. The final force could be predicted by multiplying the outputs from both lines.

1) Decoding Normalized Force Curve From Categorized MUs: The aim of this line is to decode the normalized force curve by estimating fluctuations of the muscle force. Two conjunctive approaches were designed including an electricity-to-force transformation using a physiological twitch force model and a deep network that further estimated the normalized force curve.

a) Twitch force model: This model can establish the electricity-to-force transformation process at an MU level that is essentially involved in the sEMG-based force estimation. Every occurrence of an MU discharge corresponds to the generation of a twitch. This process is well described by a twitch force model originally proposed by Milner-Brown *et al.* [31], which generally explains how a muscle force is constituted from twitch forces generated by a group of activated MUs. In this model, the force twitch is simulated as a critically damped second-order system $f(t)$:

$$f(t) = \frac{P \cdot t}{T} e^{1-(\frac{t}{T})}, \tag{1}$$

where T is the contraction time and P is the value of peak twitch force. In the original version of this model [31]–[33], P was modeled to be positively correlated with the MU size, and the contraction time T was inversely related to twitch amplitudes P. The MU size was simplified as a series of integer numbers assigned from 1 to 120 where 1 is the size of the smallest MU and 120 is the size of the largest MU in the motor neuron pool. These parameters can only reflect the relative size and relation between MUs and their force contributions. These are only meaningful in a simulation study and unavailable in practical use. An estimation of MU size is required when applying this model. Although without any prior knowledge of the recruitment order for each MU, the MU recruitment was believed to follow the *size principle* [32]. In addition, the size of an MU was reflected by the MUAP amplitude. According to the above assumption, P was modeled to be linearly correlated with the peak-to-peak amplitude of the MUAP waveform. Its value multiplied by pre-defined constant of 0.01 (just for unit conversion) was used to straightforwardly assign the peak amplitude of twitch force P. Thus, T was calculated as follows [32], [33] where TL was determined to be 300 according to some pretests:

$$T = TL \cdot \left(\frac{1}{P}\right)^{1/4.2}. \tag{2}$$

Each channel from the 8×8 array obtained a twitch force based on its own MUAP waveform forming an 8×8 array of twitch force for each MU. A 8×8 array twitch force train (TFT) was obtained through a convolution of the twitch force and corresponding discharge timing trains thus representing a basic contribution of each MU to force. One may argue that the multi-channel form is just meaningful for the MUAP waveform but it is not for the twitch force. We intentionally kept the transformed TFTs in the multi-channel form to preserve important spatial information. Therefore, it could be processed and characterized by the subsequent deep learning network into which the TFTs were fed.

The TFTs of a group of decomposed MUs from each data segment were further re-arranged and sorted according to the MU categories. By directly accumulating the TFTs of the MUs within every category, a categorized TFT (CTFT) was generated and represented by a $10000 \times 8 \times 8 \times 10$ feature matrix. Here, 10 is the number of categories; 8×8 indicates the electrode array; and 10000 represents the time length.

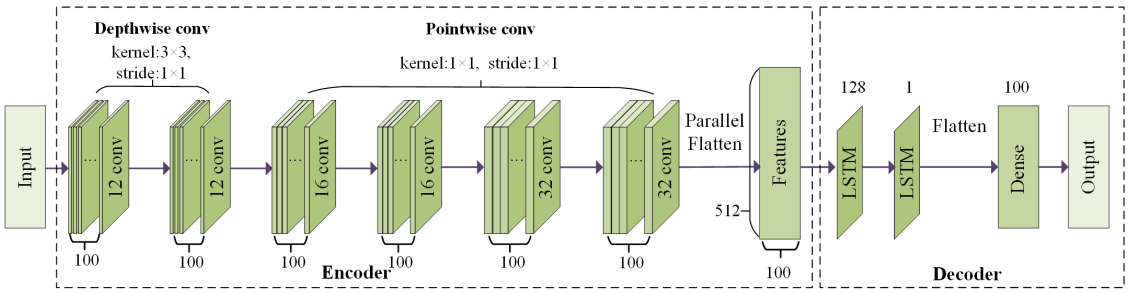

Fig. 3. Structure of the proposed encoder-decoder network. The size of the input is 100 × 10 × 8 × 8, where 100 represents a sample with length of 50ms. 10 is the MU category number and 8 × 8 is the spatial distribution of electrode. The six layers of convolution in the encoder were set at the valid padding.

b) Encoder-decoder deep network: The previous approach transformed the MU electrical activities into mechanical CTFTs grouped by 10 MU categories in a channel-wise manner. This procedure was conducted to address how and how differently these MU categories contributed to the muscle force. A deep learning network was built in an encoder-decoder manner (Fig. 3) taking advantage of characterizing the spatial information over the 2D array.

The encoder architecture was inspired by the depthwise separable convolution [34], [35]. The idea was to independently map spatial correlations (the 8 × 8 array, equivalent to width × height of an image) and cross-channel correlations (the channel refers to color channel with a dimension of 3 in natural images and 10 MU categories in this study other than the sEMG recording channel). In contrast to the original depthwise separable convolution that executes the pointwise convolution operation immediately following the depthwise convolution, two consecutive depthwise convolution layers were designed here to encode specific force contributions for each MU category from the amplitudes of MUAP waveform as well as to define the spatial distribution. In each layer, 12 filters with a filter size at 3 × 3, a stride of 1 × 1, and valid padding were performed on an individual channel of the feature map. Here the feature map is a common term representing output data structure of the prior layers. Two layers of this convolution enables an enhanced capability of spatial information characterization with a proper receptive field size at 5 × 5. Subsequently, four pointwise convolutions were adopted to extract the category correlations. Each layer of the pointwise convolutions employed 1 × 1 convolution with a stride of 1 × 1 and valid padding to be performed across channels. The filter numbers of the four layers were 16, 16, 32, and 32. A total of six layers were constructed in a parallel manner to deal with the four-dimensional input feature matrix of a sample. In each layer, 100 parallel convolution operations were employed by sharing weights between them to deal with time steps of 100. The features obtained from the encoder were then fed into the decoder. The typical long short-term memory (LSTM) [36], [37] was employed to capture the long-range dependencies of data. A two-layer LSTM block was designed to constitute the decoder. The first layer consisted of 128 memory cells and the second layer contained one memory cell. The outputs were given by a fully connected layer with 100 neurons. The above hyper-parameters were designed according to the characteristics of the input and were fine-tuned and validated through pre-tests. The architecture of the proposed deep network is summarized in Fig. 3.

The network was trained via training samples well labeled by recorded true force curves normalized between 0-1. Before feeding into the network, the CTFT from each data segment was normalized as well: The TFTs of 10 MU categories were summed up, and the maximal value of the summation over the 64 electrode channels was obtained to normalize the original CTFT. The normalized CTFT feature matrix was then further segmented into 100 samples via a non-overlapping window at a length of 50 ms (equivalent to 100 data points). Thus, every window with a $100 \times 10 \times 8 \times 8$ feature matrix was considered to be the basic sample for network training and testing. Each sample was labelled via the corresponding 100-point normalized force curve during the training phase. The network was trained using Python with the Keras framework. The mean square error (MSE) was minimized with mini-batch gradient descent [38] with a learning rate of 0.0001. When the network was well trained, it could predict a normalized force curve by every consecutive window for any input CTFT.

2) Predicting Force Gain Factor to Estimate the Actual Force: We present here the other line in the force estimation module of the proposed framework to estimate the gain factor for retrieving the actual force level. The increased force level is expected to be reflected by both recruitment of more MUs and increase in their firing frequencies according to prior physiological knowledge [32]. However, these two phenomena might not be obvious from the decomposed MUs due to unavoidable loss of partial MU information. Alternatively, it is feasible to analyze the MU category distribution of a set of decomposed MUs by inferring the straightforward force level. As each MU category was previously determined by a previous MU tracking and identification module, it was straightforward to calculate the MU category distribution here.

For a set of MUs obtained in each trial, we counted the number of MUs in every MU category. Then, it was normalized by the total number of decomposed MUs to get the proportion of MUs belonging to every category. On this basis, a center of gravity was calculated:

$$\text{Grav} = \sum_{i=1}^{10} i \cdot Pi, \tag{3}$$

where i represents the MU category and Pi is the corresponding proportion. In addition, the median value of the MU category in their distribution was calculated as well.

Both values were used to form a feature vector for each data segment/trial. These feature vectors well-labeled by their actual force levels from the training dataset, were used to construct a support vector machine model using quadratic kernel (QSVM) [39], [40]. Thus, any given feature vector could be fed into the trained model to predict a force level for the data trial. This procedure was equivalent to estimation of a corresponding gain factor, which was in turn used to amplify the normalized force (which was predicted in the previous line) so as to retrieve the actual force.

E. Model Training and Performance Evaluation

The proposed framework involved multiple supervised machine learning approaches/models that needed to be trained appropriately with labelled data to enable corresponding functions. All of these approaches were trained consistently. Besides, the framework for force estimation was tested in a user-specific manner with both the training and testing datasets from the same subject. For each subject, there were five data segments/trials at each of four force levels. Thus, a five-fold cross-validation strategy was conducted: One data segment from each of four force levels was selected respectively to form the testing dataset while the remaining 16 data segments were used for training all supervised learning models.

Two metrics were employed to evaluate the force estimation performance: root mean square deviation (RMSD) [12] and goodness of fit (R^2) from a linear regression [41] between the estimated force and the actual force. The small RMSD and the high R^2 indicate satisfactory performance. Both metrics were performed on the predicted normalized force curve, i.e., the output of the deep neural network, without consideration of the final predicted force by multiplying the predicted gain factor.

Three common methods for force estimation were selected for performance comparison. The method using a composite firing sequence of all obtained MUs [22], [23] was selected and denoted as the FR method because it is a representative MU-based method for force estimation. In this method, discharge timings from all decomposed MUs were summed up to form a composite firing sequence without consideration of different contributions of these MUs to the force. The instant firing rate was calculated by dividing the number of discharges within a sliding windows by the window length of 400 ms where the window increment was set at 50 ms [23]. The instant firing rates were regarded as the features to predict the force using the three-order polynomial regression model [12]. In addition, methods employing macroscopic sEMG amplitude- associated features were conducted as well. Both the averaged RMS [10], [11] amplitude and the envelop [12] of the sEMG signals over all channels were selected due to their wide applications. These were denoted as the RMS method and the ENV method, respectively. For the RMS method, the same overlapping sliding window was adopted to be the same as the FR method. For the ENV method, a full-wave rectification along with a 3-Hz butterworth low-pass filter was adopted to compute the envelop of each sEMG channel [12]. Similarly, the same three-order polynomial regression model [12] was applied to predict the force for both methods. For the above three methods, both the true force and their corresponding features were normalized between 0 and 1. Other settings including the training and testing strategy were the same as those in the proposed method or were optimally assigned.

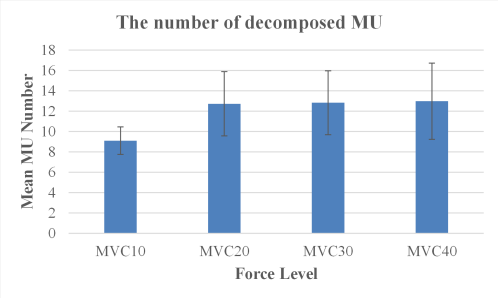

Fig. 4. The number of decomposed MUs for each force level over all subjects.

F. Statistical Analysis

A one-way ANOVA was applied to examine the effect of muscle contraction strength (10%, 20%, 30% and 40% MVC) on the number of decomposed MUs. To examine the effect of the method (four methods in total: the proposed method, the FR method, the RMS method and the ENV method) and the force level (four levels: 10%, 20%, 30% and 40% MVC) on the force estimation performance, two separate repeated-measure two-way ANOVAs were performed on the RMSD and R^2 respectively; both factors were considered as within-subject factors. If possible, post-hoc multiple pairwise comparisons with a Bonferroni correlation were conducted. The level of statistical significance was set at $p < 0.05$ for all analyses. All statistical analyses were completed using SPSS (ver. 24.0, SPSS Inc. Chicago, IL).

III. Results

A. HD-sEMG Decomposition Results

The decomposed MU number was calculated for each force level by averaging over all trials from eight subjects, giving a result at 9.10 ± 1.35 (mean ± standard deviation), 12.73 ± 3.15, 12.83 ± 3.13, and 12.98 ± 3.75 for the four force levels shown in Fig. 4, respectively. There was no significant difference ($p > 0.05$) of decomposed MU number reported between any pair of force level among MVC20, MVC30, and MVC40. However, a significant difference was reported between MVC10 and any of other force levels presenting a significant increase on the MU number for the three larger force levels.

Fig. 5 gives an example of HD-sEMG decomposition results from a representative data trial from subject 2. Each obtained MU was represented by its MUAP waveform and corresponding firing sequence. All of these decomposed MUs were produced in an uncertain order evidently. Each MU can be identified with its spatial distribution pattern of MUAP waveforms over all channels as shown in Fig. 5(b). The core

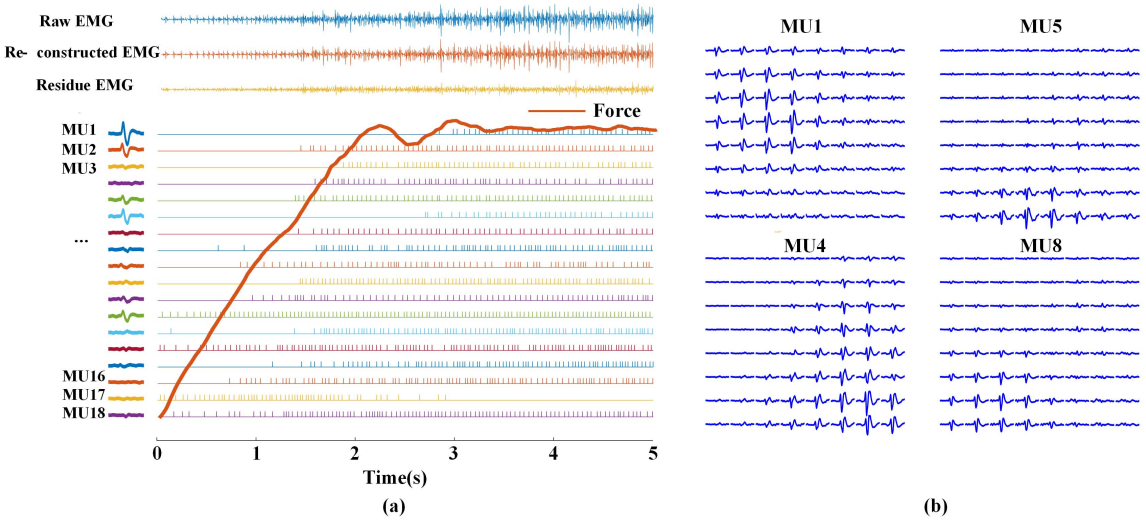

Fig. 5. (a) An example of the EMG decomposition results from a 5-s segment of subject 2. A series of MU discharge timings and corresponding MUAP waveforms from channel 37 were presented. (b) The spatial distribution of waveforms over all channels were illustrated for four representative MUs.

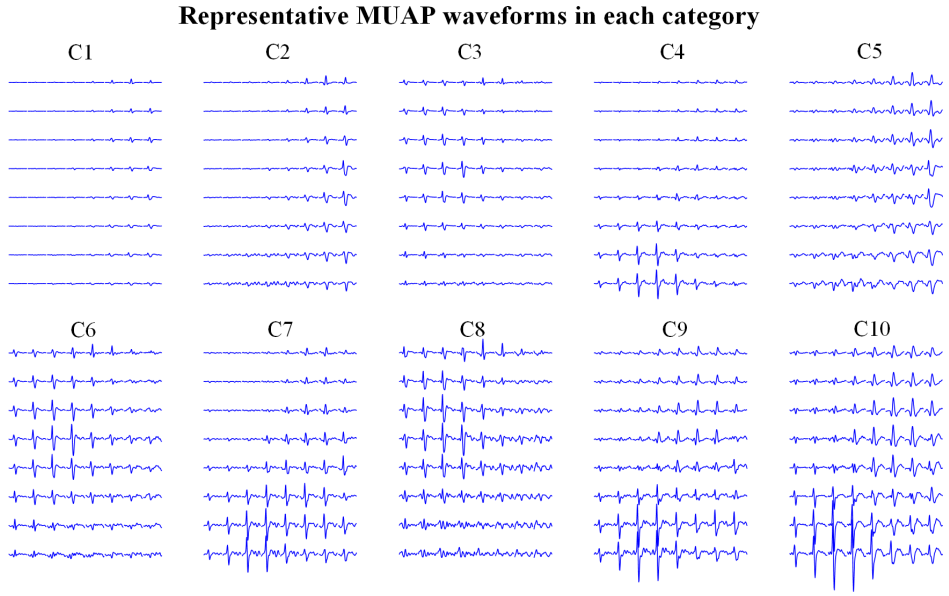

Fig. 6. Illustration of MU proportion falling into each category for all force levels and subjects.

area of channels with larger MUAP amplitudes is quite different between MU4 and MU8 in the case of the comparable maximum amplitude of their MUAP waveforms.

B. MU Identification and Tracking Results

Fig. 6. presents examples of MUAP waveforms over the 2D array of 10 representative MUs selected from 10 categories (C1-C10) in a size increasing order, respectively. Visual inspection shows that the MU in every category has a specific spatial distribution pattern of waveforms. Besides, it was found that MUAP waveform from C1 to C10 presented a gradual enlargement of amplitude. For a clearer description of the general tracking procedure, the decomposed MUs from two trials as well as its corresponding category are illustrated in Fig. 7. There were slight differences either in the total number or MUAP waveforms between both MU groups although they were at the same force level from one subject.

Fig. 7 shows that MUs clustered into the same category (e.g., C3, C4 and C9) have a proximate MUAP waveform distribution regardless of whether they are in the same trial. Specifically, different MUs with dissimilar MUAP waveforms but proximate amplitude distribution can be clustered into the same category such as some MU examples in C5 or C7.

C. Force Estimation Results

Based on the 10 predefined MU categories, the proportion of each MU category could be calculated after deriving multiple MUs from a single data trial. An example is illustrated in Fig. 8 and presents the MU category's distribution of each trial from subject 5. Although the number of MUs in each

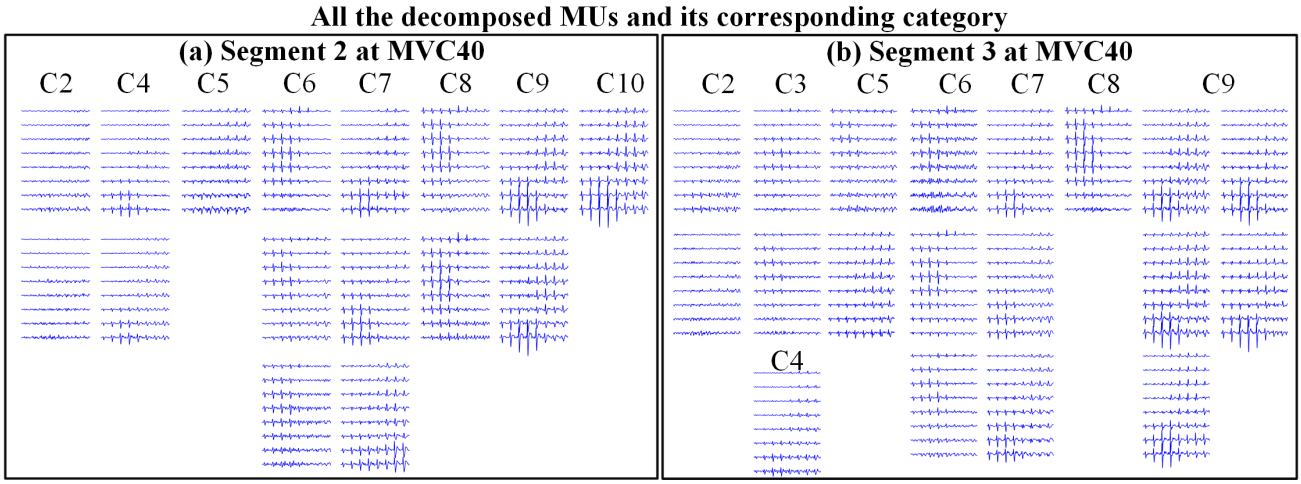

Fig. 7. All the decomposed MUs and the corresponding category for two trials selected from subject 5.

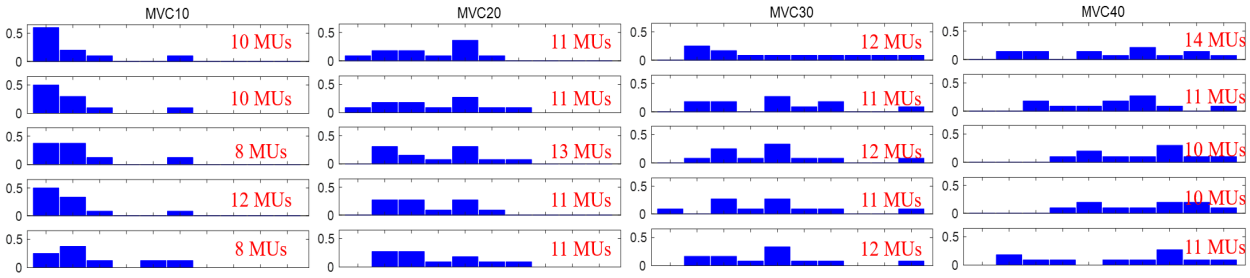

Fig. 8. Illustration of MU proportion falling into each category for all force levels of subject 5.

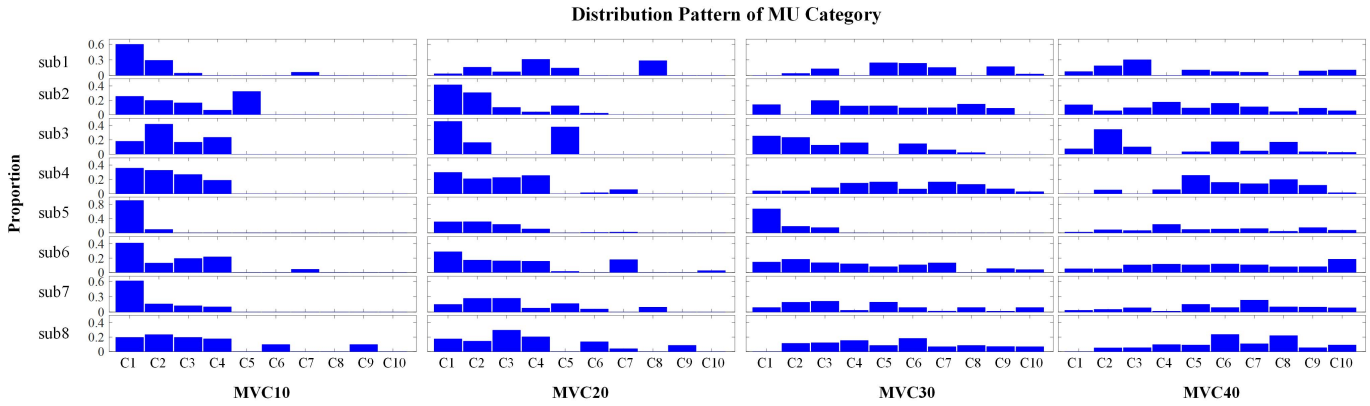

Fig. 9. Illustration of MU proportion falling into each category for all force levels and subjects.

category varied across trials within the same force level, their MU category distribution showed a very consistent pattern within the same force level but quite different patterns across force levels. Specifically, MUs with larger category number (supposed to have a larger size) gradually appeared as the force level increased. Fig. 9 further reports the MU category's distribution patterns summarized for all subjects at four force levels, respectively. The same finding can be observed in which the MU category distribution pattern can be characterized by increasing the proportion of MUs with larger amplitudes at larger force levels. Although it is difficult to discriminate force levels using the number of decomposed MUs (almost comparable across levels), the MU category distribution pattern can work.

Fig. 10 presents an estimation based on the proposed method that first tracked the force in its trend more accurately than the ENV method, the RMS method, and the FR method. The FR method using discharge properties of MUs can track subtle force fluctuations even though it reported a worse performance mainly due to a larger time delay in estimating the force curve. Visual inspection shows that the proposed method outperformed other methods and exhibited superior

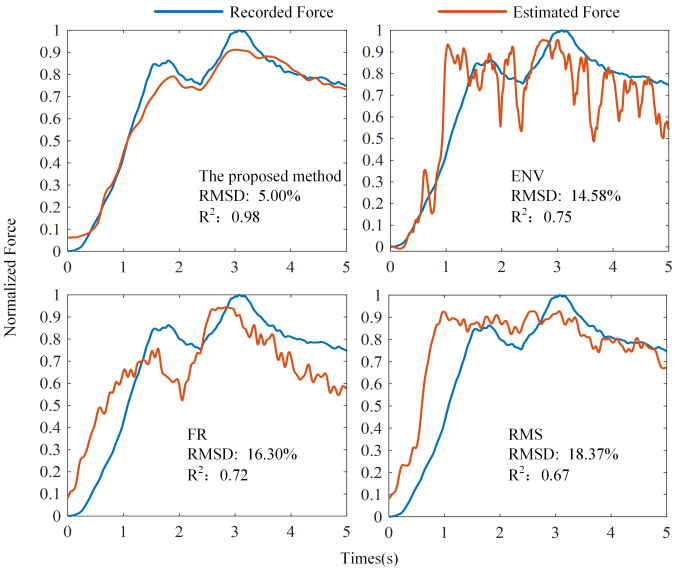

Fig. 10. Force estimation results of subject 5 at 20%MVC. The corresponding methods and its performance evaluation were presented in each subplot.

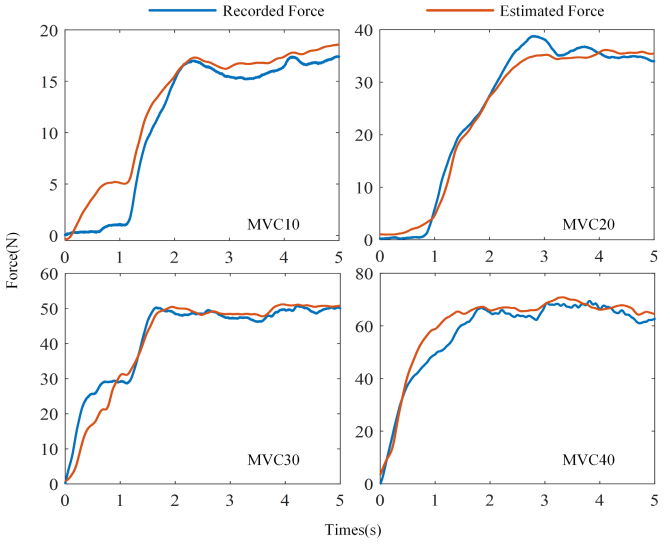

Fig. 11. Examples of predicted force segments after multiplying corresponding force gain.

performance in tracking subtle force fluctuations with a limited time/phase difference.

A further force estimation with the force gain is shown in Fig. 11. It was able to retrieve the actual force level to calibrate the predicted force resulting from the normalized input towards the actual force curve.

Fig. 12 reports the performance of force estimation in terms of both RMSD and R^2 metrics averaged over all subjects using all four methods, respectively. When all data trials were pooled together for statistical analysis, the proposed method achieved the lowest RMSD (6.84% ± 1.29%) and the highest goodness-of-fit (0.94 ± 0.04). This approach outperformed the other three methods including the ENV method (RMSD: 13.30% ± 3.36%, R^2: 0.73 ± 0.19), the FR method (RMSD: 15.51% ± 4.65%, R^2: 0.64 ± 0.26), and RMS (RMSD: 15.44% ± 4.16%, R^2: 0.66 ± 0.25) with statistical significance ($p < 0.05$) revealed by ANOVAs.

IV. Discussions

It is very challenging to interpret the MU activities after sEMG decomposition facing difficulty in cross-trial MU tracking and unavoidable loss of partial neural drive information due to incomplete decomposition. The major contribution of this study is to provide a framework of engineering solutions for addressing both issues resulting from the cutting-edge but developing sEMG decomposition technique. These solutions are presented and applied as a novel method for decoding the muscle force.

The amplitude-based method is a traditional and straightforward way for muscle force estimation. In this study, two widely used amplitude-based methods were tested, and they achieved consistent performance with previous reports [22], [23]. The FR method directly used the composite spike trains through sEMG decomposition for muscle force estimation. This method was based on the fact that a stronger central stimulation activates more MUs as well as more frequent firings of these MUs, thus generating greater muscle strength. However, this MU-based method failed to outperform traditional amplitude-based methods. We believe that the main reason may fall on the lack of differential treatment of different MUs as well as the negative effect brought from both issues mentioned above. This also indicates that processing only MU firings may not make full use of the neural drive information. In fact, relying on just the firing information is basically a simplified strategy that avoids both issues in the interpretation of MU activities. The insufficient performance of the FR method suggests the necessity of providing effective solutions to both issues. Instead, the proposed framework is dedicated to addressing both issues using two data processing modules respectively. When applied to muscle force estimation, this method significantly outperformed other common methods ($p < 0.001$), demonstrating its feasibility of the designed solutions in addressing both issues and the usability of decoding the muscle force. This confirms the anticipation of this study that addressing both issues can facilitate sufficient interpretation of the microscopic neural drive information.

In the proposed framework, the important spatial information in the form of individual MUAP waveforms distributed in the 2D grid was used to assist the identification and tracking of MUs across trials. Two benefits were obtained from this module. The first benefit is the capability of cross-trial MU tracking, which makes it possible to analyze MUs obtained from separate implementations of the sEMG decomposition algorithm on different data trials. This enables the generalization of knowledge learned from one trial to others, which is a prerequisite for introducing advanced supervised machine learning methods like deep neural networks in processing MU activities. The other benefit is to further sort the categorized MUs in size or type thus enabling the calculation of MU proportions to characterize the distribution of MU categories in each trial. MUs with larger amplitude gradually appeared with increasing proportions at greater force levels as shown

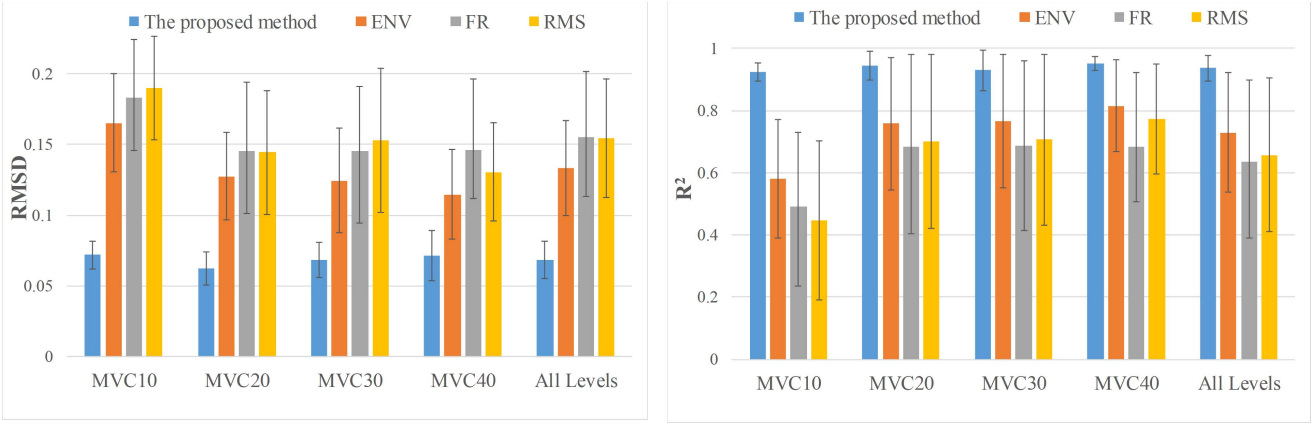

Fig. 12. Performance of force estimation evaluated by the RMSD (left) and R^2 (right) using the proposed method and three comparison methods, respectively.

in Figs. 8 and 9. This finding agrees with the *size principle* [32], and it further demonstrated the effectiveness of the MU tracking module and the subsequent muscle force gain factor prediction using the MU proportions.

It should be noted that the current study only presents a module for general MU identification and tracking. In contrast to the strict tracking and recognition of MU reported in previous work [42], it rather handled categories that contained MUs exhibiting similar spatial and amplitude characteristics. This process induced some tolerance of the MU-matching process. Such tolerance was introduced by our simple hypothesis to associate MU's function and size especially with its MUAP waveform distribution. We acknowledge that it is not truly accurate and there may be many exceptions. In the same spatial area, for instance, a deeper and stronger MU with greater force contribution could exhibit a similar MUAP waveform distribution with a smaller one above it due to the attenuation effects of the tissues. In our module, both MUs were placed into the same category and assigned by equal contributions. However, our hypothesis indicated a general trend for a population of MUs. At a given time point, it at least provided an engineering solution for modeling the function and force contributions from a group of MUs, thus ensuring computational practicability. Its successful application in this study demonstrated the feasibility of this module, and further verified the first hypothesis from the engineering point of view. Taking this advantage, in the subsequent procedure using a muscle twitch force model, the MUs' contributions to the force were directly accumulated in the same category whereas the contributions of MUs from different categories were processed differently. In addition, this MU tracking module could categorize an uncertain number of MUs from the sEMG decomposition to obtain a fixed number of size-ordered categories (Fig. 7), which served as a procedure for data regularization and dimension alignment. This is also in favor of the implementation of subsequent supervised machine learning methods.

Taking advantage of the distribution pattern of MU category to predict a gain factor is only a part of the solution to address the issue of unavoidable loss of partial neural drive information. Machine learning methods (i.e., the deep network in this study) are necessary when making use of information from the representative subset of activated MUs to estimate the function (force generation) of all activated MUs. In particular, this network focuses on characterizing the MU's spatial information compared to other MU-based methods. Taking the spatial information into account is also an important factor in the differentiation of contributions to force for different MUs. All of these features explain why the proposed method outperformed other MU-based methods.

However, there are still some limitations in this paper. The proposed framework was established to address the difficulty in the interpretation of the decomposed MU activities due to the limited performance of the current sEMG decomposition technique. As a result, it involves relatively complex approaches. The framework can be further simplified in the future when the sEMG decomposition technique is sufficiently advanced. In addition, it was validated through an experiment conducted in limited scenarios. More factors closer to practical situations should be considered. For example, the quality of sEMG signals has a great impact on the ability of decomposition, restricting its application at high force levels. This brings a limitation wherein small-to-medium force levels were adopted rather than high force levels due to limited decomposition performance. Therefore, the estimation of the gain factor was simplified as a classification task under the current force levels. Future work will use data with sufficiently varying force levels. In this case, a regression-based method would be more appropriate in practical use to predict the current force levels. A reliable real-time decomposition algorithm and a real-time force estimation framework can guide the direction of our future work. In addition, the current study solved the one-dimensional force decoding from MU activities. Future efforts would be made to decode a more complex multi-dimensional information of motor intentions especially for simultaneous and proportional control of multiple DoFs towards future advanced applications.

More importantly, the robustness of the method against electrode shift or other interference are required for practical muscle-machine interfaces. Many previous studies have made great efforts to deal with electrode shifts or anomaly motion rejection in the scene of gesture recognition [49]–[51].

These works can offer practical experience of utilizing the spatial information to build more robust models against variations like electrode shift. Future efforts will be made towards this direction.

V. Conclusion

This study presents a novel framework that offered practical solutions to address both the cross-trial MU tracking issue and unavoidable loss of partial neural drive information issue for processing individual MU activities when applying sEMG decomposition techniques. The goal was better interpretation of the microscopic neural drive information, and the method was evolved for precise muscle force estimation. The proposed method significantly outperformed other common methods including routine sEMG amplitude-based methods or a representative MU-based method demonstrating its effectiveness. This study offers valuable solutions to both technical issues in interpreting complex microscopic neural drive information raised from the application of sEMG decomposition. Our efforts will promote the usability of sEMG decomposition techniques towards advanced decoding of motor intentions.

References

[1] R. Zhang *et al.*, "An EOG-based human–machine interface to control a smart home environment for patients with severe spinal cord injuries," *IEEE Trans. Biomed. Eng.*, vol. 66, no. 1, pp. 89–100, Jan. 2019.

[2] J. Zhang, B. Wang, C. Zhang, Y. Xiao, and M. Y. Wang, "An EEG/EMG/EOG-based multimodal human-machine interface to real-time control of a soft robot hand," *Frontiers Neurorobot.*, vol. 13, p. 7, Mar. 2019.

[3] A. Neto, W. Celeste, V. Martins, T. B. Filho, and M. Filho, "Human-machine interface based on electro-biological signals for mobile vehicles," in *Proc. IEEE Int. Symp. Ind. Electron.*, Jul. 2006, p. 2954.

[4] L. Bi, A. G. Feleke, and C. Guan, "A review on EMG-based motor intention prediction of continuous human upper limb motion for human-robot collaboration," *Biomed. Signal Process. Control*, vol. 51, pp. 113–127, May 2019.

[5] X. Zhang, X. Chen, Y. Li, V. Lantz, K. Wang, and J. Yang, "A framework for hand gesture recognition based on accelerometer and EMG sensors," *IEEE Trans. Syst., Man, Cybern. A, Syst., Humans*, vol. 41, no. 6, pp. 1064–1076, Nov. 2011.

[6] X. Zhang and P. Zhou, "High-density myoelectric pattern recognition toward improved stroke rehabilitation," *IEEE Trans. Biomed. Eng.*, vol. 59, no. 6, pp. 1649–1657, Jun. 2012.

[7] D. B. Chaffin, M. Lee, and A. Freivalds, "Muscle strength assessment from EMG analysis," *Med. Sci. Sports Exerc.*, vol. 12, no. 3, pp. 205–211, 1980.

[8] M. I. Polkey, M. Green, and J. Moxham, "Measurement of respiratory muscle strength," *Thorax*, vol. 50, no. 11, pp. 1131–1135, Nov. 1995.

[9] G. Drost, D. F. Stegeman, B. G. M. van Engelen, and M. J. Zwarts, "Clinical applications of high-density surface EMG: A systematic review," *J. Electromyogr. Kinesiol.*, vol. 16, pp. 586–602, Dec. 2006.

[10] E. A. Clancy and N. Hogan, "Probability density of the surface electromyogram and its relation to amplitude detectors," *IEEE Trans. Biomed. Eng.*, vol. 46, no. 6, pp. 730–739, Jun. 1999.

[11] N. Hogan and R. W. Mann, "Myoelectric signal processing: Optimal estimation applied to electromyography—Part II: Experimental demonstration of optimal myoprocessor performance," *IEEE Trans. Biomed. Eng.*, vol. BME-27, no. 7, pp. 396–410, Jul. 1980.

[12] C. Huang, X. Chen, S. Cao, B. Qiu, and X. Zhang, "An isometric muscle force estimation framework based on a high-density surface EMG array and an NMF algorithm," *J. Neural Eng.*, vol. 14, no. 4, Aug. 2017, Art. no. 046005.

[13] X. Zhang, D. Wang, Z. Yu, X. Chen, S. Li, and P. Zhou, "EMG-torque relation in chronic stroke: A novel EMG complexity representation with a linear electrode array," *IEEE J. Biomed. Health Informat.*, vol. 21, no. 6, pp. 1562–1572, Nov. 2017.

[14] F. Mobasser, J. M. Eklund, and K. Hashtrudi-Zaad, "Estimation of elbow-induced wrist force with EMG signals using fast orthogonal search," *IEEE Trans. Biomed. Eng.*, vol. 54, no. 4, pp. 683–693, Apr. 2007.

[15] M. Chen, A. Holobar, X. Zhang, and P. Zhou, "Progressive FastICA peel-off and convolution kernel compensation demonstrate high agreement for high density surface EMG decomposition," *Neural Plasticity*, vol. 2016, pp. 1–5, Aug. 2016.

[16] M. Chen, X. Zhang, X. Chen, and P. Zhou, "Automatic implementation of progressive FastICA peel-off for high density surface EMG decomposition," *IEEE Trans. Neural Syst. Rehabil. Eng.*, vol. 26, no. 1, pp. 144–152, Jan. 2018.

[17] M. Chen and P. Zhou, "A novel framework based on FastICA for high density surface EMG decomposition," *IEEE Trans. Neural Syst. Rehabil. Eng.*, vol. 24, no. 1, pp. 117–127, Jan. 2016.

[18] A. Holobar, D. Farina, M. Gazzoni, R. Merletti, and D. Zazula, "Estimating motor unit discharge patterns from high-density surface electromyogram," *Clin. Neurophysiol.*, vol. 120, no. 3, pp. 551–562, 2009.

[19] C. Chen, G. Chai, W. Guo, X. Sheng, D. Farina, and X. Zhu, "Prediction of finger kinematics from discharge timings of motor units: Implications for intuitive control of myoelectric prostheses," *J. Neural Eng.*, vol. 16, no. 2, Apr. 2019, Art. no. 026005.

[20] C. Chen *et al.*, "Hand gesture recognition based on motor unit spike trains decoded from high-density electromyography," *Biomed. Signal Process. Control*, vol. 55, Jan. 2020, Art. no. 101637.

[21] C. K. Thompson *et al.*, "Robust and accurate decoding of motoneuron behaviour and prediction of the resulting force output," *J. Physiol.*, vol. 596, no. 14, pp. 2643–2659, Jul. 2018.

[22] D. Farina *et al.*, "Man/machine interface based on the discharge timings of spinal motor neurons after targeted muscle reinnervation," *Nature Biomed. Eng.*, vol. 1, no. 2, pp. 1–12, Feb. 2017.

[23] C. Dai, Y. Zheng, and X. Hu, "Estimation of muscle force based on neural drive in a hemispheric stroke survivor," *Frontiers Neurol.*, vol. 9, p. 187, Mar. 2018.

[24] R. Istenic, A. Holobar, R. Merletti, and D. Zazula, "EMG based muscle force estimation using motor unit twitch model and convolution kernel compensation," in *Proc. 11th Medit. Conf. Med. Biol. Eng. Comput.*, 2007, pp. 114–117.

[25] X. Tang, X. Zhang, X. Gao, X. Chen, and P. Zhou, "A novel interpretation of sample entropy in surface electromyographic examination of complex neuromuscular alternations in subacute and chronic stroke," *IEEE Trans. Neural Syst. Rehabil. Eng.*, vol. 26, no. 9, pp. 1878–1888, Sep. 2018.

[26] D. Arthur and S. Vassilvitskii, "K-means plus plus: The advantages of careful seeding," in *Proc. 18th Annu. ACM-Siam Symp. Discrete Algorithms*, 2007, pp. 1027–1035.

[27] X. Huang, Y. Ye, and H. Zhang, "Extensions of kmeans-type algorithms: A new clustering framework by integrating intracluster compactness and intercluster separation," *IEEE Trans. Neural Netw. Learn. Syst.*, vol. 25, no. 8, pp. 1433–1446, Aug. 2014.

[28] K. Krishna and M. N. Murty, "Genetic K-means algorithm," *IEEE Trans. Syst. Man, Cybern. B, Cybern.*, vol. 29, no. 3, pp. 433–439, Jun. 1999.

[29] P. Bholowalia and A. Kumar, "EBK-means: A clustering technique based on elbow method and k-means in WSN," *Int. J. Comput. Appl.*, vol. 105, no. 9, pp. 17–24, 2014.

[30] M. A. Syakur, B. K. Khotimah, E. M. S. Rochman, and B. D. Satoto, "Integration K-means clustering method and elbow method for identification of the best customer profile cluster," in *Proc. 2nd Int. Conf. Vocational Educ. Electr. Eng. (ICVEE)*, vol. 336, 2018, Art. no. 012017.

[31] H. S. Milner-Brown, R. B. Stein, and R. Yemm, "The contractile properties of human motor units during voluntary isometric contractions," *J. Physiol.*, vol. 228, no. 2, pp. 285–306, Jan. 1973.

[32] A. J. Fuglevand, D. A. Winter, and A. E. Patla, "Models of recruitment and rate coding organization in motor-unit pools," *J. Neurophysiol.*, vol. 70, no. 6, pp. 2470–2488, Dec. 1993.

[33] P. Zhou, N. L. Suresh, and W. Z. Rymer, "Model based sensitivity analysis of EMG–force relation with respect to motor unit properties: Applications to muscle paresis in stroke," *Ann. Biomed. Eng.*, vol. 35, no. 9, pp. 1521–1531, Aug. 2007.

[34] A. G. Howard *et al.*, "MobileNets: Efficient convolutional neural networks for mobile vision applications," 2017, *arXiv:1704.04861*.

[35] F. Chollet, "Xception: Deep learning with depthwise separable convolutions," in *Proc. IEEE Conf. Comput. Vis. Pattern Recognit. (CVPR)*, Jul. 2017, pp. 1800–1807.

[36] S. Hochreiter and J. Schmidhuber, "Long short-term memory," *Neural Comput.*, vol. 9, no. 8, pp. 1735–1780, 1997.

[37] F. A. Gers, "Learning to forget: Continual prediction with LSTM," in *Proc. 9th Int. Conf. Artif. Neural Netw., (CANN)*, Oct. 1999, pp. 850–855.

[38] M. Li, T. Zhang, Y. Chen, and A. J. Smola, "Efficient mini-batch training for stochastic optimization," in *Proc. 20th ACM SIGKDD Int. Conf. Knowl. Discovery Data Mining*, Aug. 2014, pp. 661–670, doi: 10.1145/2623330.2623612.

[39] I. Dagher, "Quadratic kernel-free non-linear support vector machine," *J. Global Optim.*, vol. 41, no. 1, pp. 15–30, May 2008.

[40] D. H. Hong and C. Hwang, "Interval regression analysis using quadratic loss support vector machine," *IEEE Trans. Fuzzy Syst.*, vol. 13, no. 2, pp. 229–237, Apr. 2005.

[41] R. L. Eubank and C. H. Spiegelman, "Testing the goodness of fit of a linear-model via nonparametric regression techniques," *J. Amer. Stat. Assoc.*, vol. 85, no. 410, pp. 387–392, Jun. 1990.

[42] E. Martinez-Valdes, F. Negro, C. M. Laine, D. Falla, F. Mayer, and D. Farina, "Tracking motor units longitudinally across experimental sessions with high-density surface electromyography," *J. Physiol.*, vol. 595, no. 5, pp. 1479–1496, Mar. 2017.

[43] T. Kapelner, F. Negro, O. C. Aszmann, and D. Farina, "Decoding motor unit activity from forearm muscles: Perspectives for myoelectric control," *IEEE Trans. Neural Syst. Rehabil. Eng.*, vol. 26, no. 1, pp. 244–251, Jan. 2018.

[44] A. D. Vecchio and D. Farina, "Interfacing the neural output of the spinal cord: Robust and reliable longitudinal identification of motor neurons in humans," *J. Neural Eng.*, vol. 17, no. 1, Feb. 2020, Art. no. 016003.

[45] C. Chen, S. Ma, X. Sheng, D. Farina, and X. Zhu, "Adaptive real-time identification of motor unit discharges from non-stationary high-density surface electromyographic signals," *IEEE Trans. Biomed. Eng.*, vol. 67, no. 12, pp. 3501–3509, Dec. 2020.

[46] A. Hyvärinen, "Fast and robust fixed-point algorithms for independent component analysis," *IEEE Trans. Neural Netw.*, vol. 10, no. 3, pp. 626–634, May 1999.

[47] A. K. Clarke *et al.*, "Deep learning for robust decomposition of high-density surface EMG signals," *IEEE Trans. Biomed. Eng.*, vol. 68, no. 2, pp. 526–534, Feb. 2021.

[48] M. Lukács, L. Vécsei, and S. Beniczky, "Large motor units are selectively affected following a stroke," *Clin. Neurophysiol.*, vol. 119, no. 11, pp. 2555–2558, Nov. 2008.

[49] L. Wu, X. Zhang, K. Wang, X. Chen, and X. Chen, "Improved high-density myoelectric pattern recognition control against electrode shift using data augmentation and dilated convolutional neural network," *IEEE Trans. Neural Syst. Rehabil. Eng.*, vol. 28, no. 12, pp. 2637–2646, Dec. 2020.

[50] X. Zhang, L. Wu, B. Yu, X. Chen, and X. Chen, "Adaptive calibration of electrode array shifts enables robust myoelectric control," *IEEE Trans. Biomed. Eng.*, vol. 67, no. 7, pp. 1947–1957, Jul. 2020.

[51] E. J. Scheme, B. S. Hudgins, and K. B. Englehart, "Confidence-based rejection for improved pattern recognition myoelectric control," *IEEE Trans. Biomed. Eng.*, vol. 60, no. 6, pp. 1563–1570, Jun. 2013.

[52] X. Hu, W. Z. Rymer, and N. L. Suresh, "Motor unit pool organization examined via spike-triggered averaging of the surface electromyogram," *J. Neurophysiol.*, vol. 110, no. 5, pp. 1205–1220, May 2012.

[53] C. A. Knight and G. Kamen, "Superficial motor units are larger than deeper motor units in human vastus lateralis muscle," *Muscle Nerve*, vol. 31, no. 4, pp. 475–480, 2005.